ORIGINAL ARTICLE

lajss.org© Latin American Journal of Solids and Structures

www.lajss.org

Mechanical Property Test and Damage Evaluation Analysis of Steel Fiber Stainless-Steel Reinforced Concrete Beams (SFSRCBs) under Impact Load

Xiwu Zhou[a], Bo Wang[a*], Xiaolu Deng[b], Jingdong Liu[a], Wen Zhang[a]

[a] School of Transportation and Civil Engineering & Architecture, Foshan University, Foshan, P.R. China. E-mail: 408680014@qq.com, bowang1127@163.com, 1067831329@qq.com, 3329786695@qq.com

[b] Western Guangdong branch, China Construction Third Bureau Group South China Co, Ltd, Guangzhou, China. E-mail: dengxl100@foxmail.com

*Corresponding author

https://doi.org/10.1590/1679-78257131

Abstract

In this paper, the ultra-high drop hammer impact test system is adopted for the vertical impact experiment on six SFSRCBs with steel fiber volume fraction of 2.0% and build the relevant numerical model. The research variables mainly include impact energy, impact mass and cumulative impact mode. The results show that, under a single equal energy impact, with the increase of the impact speed, the crack distribution of the specimen gradually tends to the mid-span local position. Compared with the impact mass, the impact speed has a greater effect on the failure mode, deformation resistance and deformation recovery ability of SFSRCBs. When the total cumulative impact energy is the same as the single impact energy, then the overall damage of the specimen caused by high-mass low-velocity cumulative impact is less significant than that caused by low-mass high-velocity cumulative impact. Combined with the finite element analysis, the calculation formula of the maximum deflection of SFSRCB under impact load is obtained. Finally, the calculation method of the impact damage evaluation factor of SFSRCBs is proposed.

Keywords

impact load; SFSRCBs; stainless steel reinforcement; mechanical properties; damage evaluation

Graphical Abstract

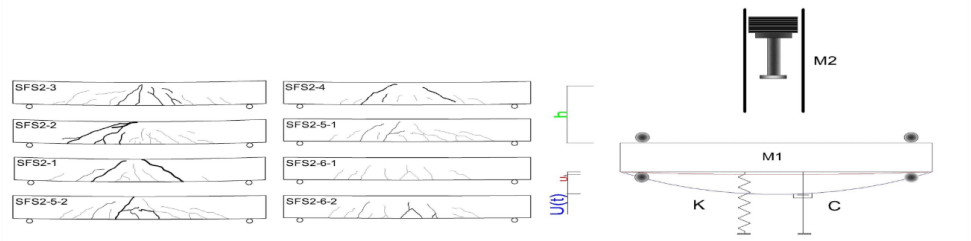

Received: May 28, 2022. In revised form: May 31, 2022. Accepted: June 05, 2022. Available online: June 10, 2022
https://doi.org/10.1590/1679-78257131

1 INTRODUCTION

Reinforced concrete structures are prone to corrosion when applied in marine environments and are frequently impacted by goods falling and ships berthing during service, thus resulting in partial or overall collapse of buildings due to loss of load-bearing balance (Zhang and Su, 2020). The impact load has the characteristics of high energy and short duration, and the incorporation of steel fiber and stainless steel can enhance the overall toughness and corrosion resistance of the component (Zhang et al., 2017). therefore, it is of great significance to study the impact resistance mechanical properties of steel fiber stainless-steel reinforced concrete beam.

At present, the research on ship-bridge collision mainly focuses on the impact resistance mechanical properties of reinforced concrete(RC) structures. For example, the influence of impact mass, impact velocity, cumulative impact times and other factors on the impact force, structural deformation and failure mode of concrete structures (Song et al., 2021; Fu et al., 2020; Xu and Zeng, 2015). At the same time, some scholars have carried out research on the impact resistance mechanical properties of stainless steel reinforced concrete (SRC) structures, Zhang et al.(2017), and Zhang and Xu.(2017a) conducted transverse impact test on SRC piers. The study results indicated that the damage degree of SRC piers was lower than that of RC piers under the same impact energy, while SRC piers had strong ductility, energy absorption capacity and impact resistance under impact load. Wu and Xu.Wu et al. (2020), based on the drop hammer impact test, measured the acceleration of the pier after impact damage, the displacement of the top, the strain of reinforcement, rotation of the pier bottom and derivation and development of the surface cracks of the specimen, and comprehensively analyzed the damage degree of the pier after impact. Rabi et al. (2019) used the Continuous Strength Method (CSM), combined with relevant numerical simulations to conduct parameter research and analysis, and proposed an equation that can predict the flexural bearing capacity of SFSRC structures in engineering. Zhou et al. (2020,2019) carried out drop hammer impact test on stainless steel longitudinal bars of equal section and equal strength instead of RC beams. The study results showed that the deformation resistance and impact stiffness of SRC beams had been greatly improved, when the reinforcement ratio of SRC beams was increased and the impact energy was excessively high, then the brittle characteristics of concrete were more prominent.

At present, in view of the problem that RC structures are prone to brittleness under impact loads, some researchers have increased the toughness of components by adding fibers to the concrete. Leppanen et al. (2020) conducted numerical simulation of drop hammer impact test on RC beams and fiber reinforced concrete beams. The results showed that the addition of fiber reduced the crack spacing, crack width and mid-span deflection of the beam, while the reinforcement strain tended to be localized, and could be used to predict the risk rate of reinforcement fracture. Ulzurrun and Zanuy (2017) studied the influence of steel fiber volume fraction on the dynamic mechanical properties of reinforced concrete beams without web reinforcement using the drop hammer impact test system. The results showed that the addition of steel fiber had significantly improved the bending properties of reinforced concrete beams without web reinforcement. Dou et al. (2015) performed dynamic experimental research on SFRC beams with different steel fiber volume parameters and stirrup ratios. The study results showed that the addition of steel fiber made the cracks of reinforced concrete develop intensively, reduced the width of cracks and improved the utilization rate of stirrups. Lee et al. (2018) used a combination of experiments and numerical simulations to study SFRC beams under different impact speeds.The study results showed that the addition of steel fiber improved the impact bearing capacity and energy absorption capacity of the beam, and reduced the peak displacement and residual displacement in the midspan of the specimen. In conclusion, based on the research on the impact resistance of RC beams, the issues of easy corrosion and insufficient toughness of RC beams can be resolved by introducing stainless steel reinforcement and steel fiber. However, collision accidents often bear the characteristics of high energy and short duration, and engineering structures typically

face corrosion problems in marine environments. Therefore, it is necessary to study the impact resistance mechanical properties of SFSRCBs on the basis of solving the corrosion of reinforcement.

Furthermore, scholars both in China and internationally have performed much research on impact damage evaluation of RC structures. Tachibana et al. (2010) and Kishi et al. (2001) proposed empirical formulas for calculating the maximum mid-span deflection and residual deflection of RC beams under impact load. Zhao and Yi (2015), based on the momentum theorem and considering the beam-hammer mass ratio, created a formula and method for calculating the maximum mid-span deflection suitable for ordinary small beams. Li et al. (2020) applied experimental and numerical analysis methods to simulate the impact scenario of vehicles on piers, and proposed the residual displacement of impact point as the criterion for evaluating the impact resistance of RC piers. In order to intuitively reflect the damage distribution of the beam in the longitudinal direction, Zhao et al. (2019) established a numerical model of reinforced concrete beam under impact, and proposed a damage evaluation method based on section damage factor. In summary, the research on methods to evaluate damage of structures under impact load performed around the world mainly takes plastic deformation as the reference basis, while ignoring the elastic part of beam impact. Therefore, the damage evaluation based combining elastic and plastic deformation has not yet been thoroughly studied.

In the early stage, Zhou et al. (2021) explored the variables of steel fiber volume fraction and impact velocity of SFSRCBs under drop hammer impact. It was found that, after adding steel fiber to SRC beam, the overall energy consumption capacity of the beam body was significantly improved and the local damage of beam was effectively restrained. When the fiber content was 2.0%, the impact resistance of beam reached the maximum, and the increase of impact velocity had an impact on the transformation of failure mode of the SFSRCBs. On this basis, the drop hammer impact test on six SFSRCBs with steel fiber volume fraction of 2.0% was carried out, focusing on the influence of impact mass, single equal energy impact and cumulative impact mode (high-mass/low-velocity and low-mass/high-velocity cumulative impact) on the dynamic mechanical properties of SFSRCBs. In addition, the finite element model of SFSRCBs under drop hammer impact was established, the test results and finite element data were analyzed, and a method to evaluate damage of SFSRCBs under impact load was proposed, thereby providing theoretical support for the impact resistance design of SFSRCB on sea-crossing bridge.

2 GENERAL SITUATION OF TEST

2.1 Specimen design

A total of six steel fiber stainless steel reinforced concrete beams are designed in this test. The reinforcement method is the same (as shown in Fig. 1), and the fiber volume fraction is 2.0%. The design total length of each beam is 2,300 mm, the clear span is 2,000 mm, the section size $\mathrm{b}\times\mathrm{h}=150\mathrm{mm}\times300\mathrm{mm}$, the shear span ratio is 3.8, the design shear bearing capacity is 252.18 kN, and the bending bearing capacity is 104.64 kN. The shear-to-bending deformation ratio is converted according to the *Code for Design of Concrete Structures*, GB 50010-2010 (2015). The design strength of concrete is C40, and the thickness of the reinforcement cover is 25 mm. S2304 duplex stainless steel reinforcement (UGIGRIP1.4362) produced by UGITECH is adopted for the longitudinal bars and stirrups. The reinforcement ratio of tensile longitudinal bars is 0.89%, and the stirrup ratio is 0.67%. The reinforcement material properties measured by hydraulic servo universal testing machine (model: WAW-2000) are shown in Table 1. In the table, the yield strength of stainless steel reinforcement is the stress value when its residual strain is 0.2%. The steel fiber used in the test is consistent with that of Zhou et al.(2021).

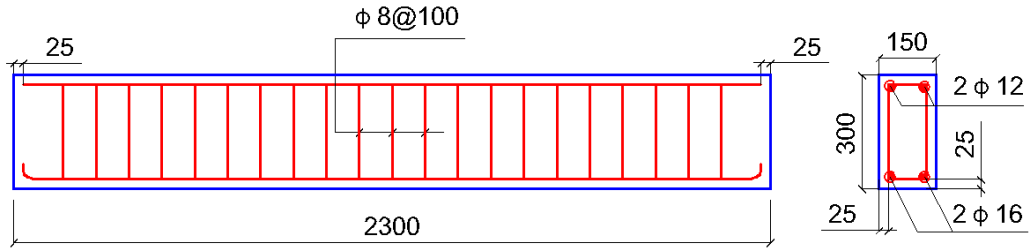

Fig. 1 Diagram of beam reinforcement (mm)

Table 1 Properties of reinforcement materials

Reinforcement category	Modulus of elasticity (10^5MPa)	Yield strength (MPa)	Ultimate strength (MPa)
stainless steel reinforced S2304	1.95	893	1051

2.2 Design of test device and test process

In this test, the advanced ultra-high heavy multifunctional drop hammer impact test system is used to conduct mid-span vertical impact on six SFSRCBs. The hammer head is a cylinder with a diameter of 200 mm. The test device is shown in Fig. 2. Both ends of the beam are simply supported. In order to prevent the two ends of the beam from jumping up and separating from the support during the impact process, a pressing plate is set at the beam top above the support, while a certain tension is applied through the pull rod to fasten the beam and the support. During the test, the fixture is loosened to release the drop hammer at the specified height, then a free fall impact specimen is made along the guide rail. The test data acquisition instrument adopts NIPXIe-1085 produced by National Instruments Co., Ltd. to acquire the impulse response data, and the maximum acquisition frequency can reach 10MHz. The test mainly studies the influence of impact energy on the dynamic mechanical properties of SFSRCBs, and the specimens are divided into three groups, A, B and C, described in detail as follows. Group A (SFS2-1, SFS2-2 and SFS2-3): a single mid-span impact load with equal energy; Group B (SFS2-5, SFS2-4 and SFS2-2): the impact mass increases in turn; Group C (SFS2-5 and SFS2-6): the impact velocity and impact mass change, two loads accumulate, and the total energy is equal to that of SFS2-4, respectively corresponding to the influence of the change in equal energy, impact mass and cumulative impact conditions on the dynamic mechanical properties of SFSRCBs. See Table 2 for the test scheme.

Table 2 Test design

Specimen No.	Fiber content (%)	Drop hammer height (m) /number of impacts	Impact mass (kg)	Measured impact velocity (m/s)	Impact energy (J)	Cumulative impact energy (J)
SFS2-1	2.0	3.0/1	400	7.66	11735.12	11735.12
SFS2-2		2.0/1	600	6.21	11569.23	11569.23
SFS2-3		1.5/1	800	5.38	11577.16	11577.16
SFS2-4		2.0/1	400	6.14	7677.81	7677.81
SFS2-5		2.0+2.0/2	200	6.22	3868.84	7737.68
SFS2-6		1.0+1.0/2	400	4.34	3767.12	7534.24

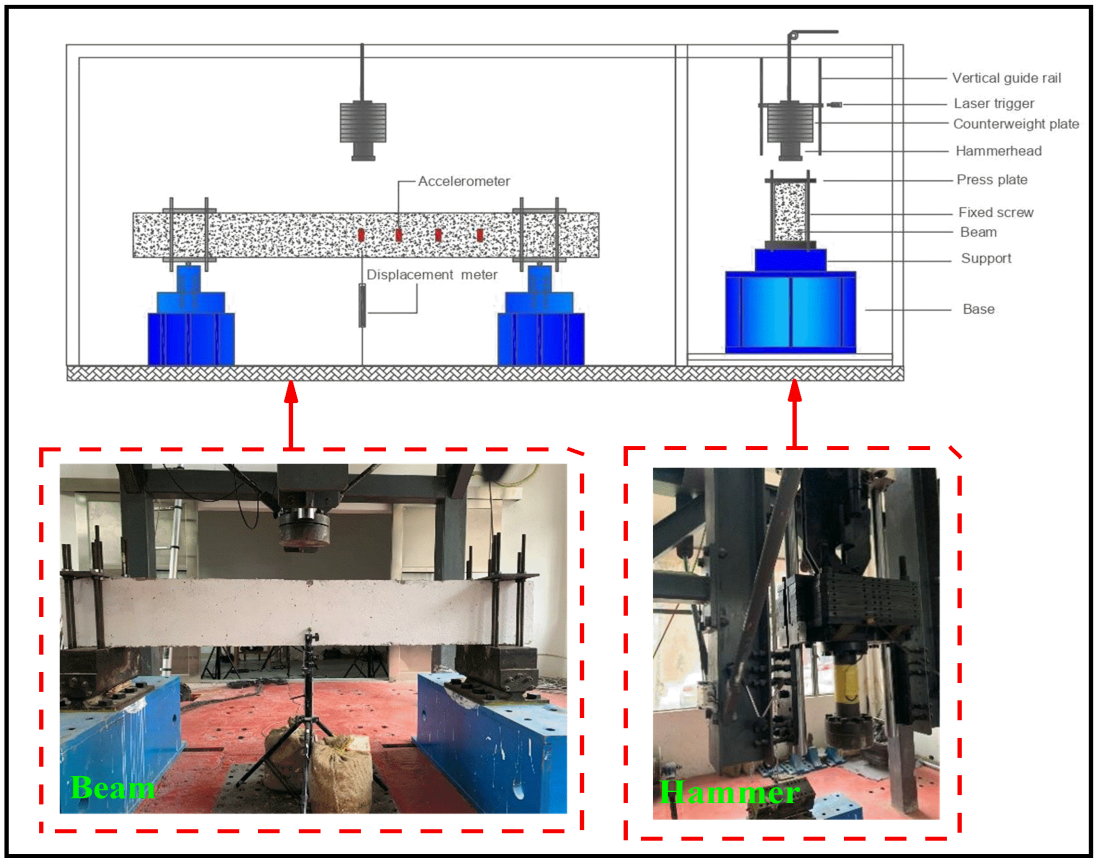

Fig. 2 Device of drop hammer impact test

3 ANALYSIS OF TEST RESULTS

3.1 Dynamic damage mechanism of SFSRCB

The damage and failure of SFSRCB under impact load is accompanied by rather complex nonlinear behavior. To thoroughly study the dynamic damage and failure mechanism of the SFSRCB, the specimen SFS2-1 beam is taken as an example to comprehensively analyze the time history of impact force, mid-span displacement and longitudinal reinforcement strain during the test, , In addition, the damage and cracking process of the specimen is drawn, as shown in Fig. 3. It can be seen from figurethat the dynamic damage process of the SFSRCB can be divided into three stages, with time as the segmentation point.

The first stage: local resistance stage (AB section: 0–1.76 ms). At the moment of contact between the drop hammer and beam, the impact force rises sharply, then decreases rapidly, so as to form a main peak value. The peak value is related to the local stiffness and impact energy of the beam-hammer contact area (Li et al., 2019). Under the action of the main peak value of the impact force on the beam body, the beam immediately obtains a downward acceleration, while simultaneously generating an upward inertial force. In the local response stage, the impact force is basically resisted by the inertial force (Li et al., 2020). Therefore, due to the existence of inertial effect, the beam basically does not deform at this stage, and the mid-span displacement and longitudinal reinforcement strain respond only minimally. At this stage, the beam only produces several fine cracks directly below the impact point, beginning at the bottom of the beam.

The second stage: overall deformation stage (BC section: 1.76–16 ms). After the beam collides with the hammer, the kinetic energy of the hammer head is transferred into the beam body. Next, the beam body acquires a velocity and

begins to move downward, the mid-span displacement gradually rises, the tensile strain of the longitudinal reinforcement at the bottom of the beam gradually increases, and the compressive strain of the longitudinal reinforcement at the top of the beam also gradually increases. When the mid-span displacement reaches the peak at 16 ms, the strain of the longitudinal reinforcement at the top and bottom of the beam basically reaches the peak, thus indicating that energy dissipation of reinforcement deformation is a very important impact energy dissipation mechanism of the beams (Liu et al., 2015). At this stage, the impact force basically tends toward a constant platform value after a period of vibration, and this platform value is related to the overall stiffness of the specimen (Cai et al., 2019). The response of the beam body mainly includes the extension and development of the original micro cracks in the mid-span area. Several micro-oblique cracks are produced in the shear span area, and the increase of crack width is not as significant as that in the mid-span area. Finally, when the mid-span displacement reaches the peak, the specimen is damaged most seriously.

The third stage: rebound stage (CD section: 16–24.09 ms). After 16 ms, the momentum becomes a dissipation process, thus the beam-hammer separation is inevitable, and the impact force gradually decreases until it approaches 0. The mid-span displacement gradually decreases to a certain extent, then tends to a constant value, thus forming a residual displacement. The strain of longitudinal reinforcement at the top and bottom of the beam gradually decreases, and the yield of the tensile reinforcement at the bottom can be observed. At this stage, the cracks on the beam surface are closed, and a small amount of concrete is peeled off in the beam-hammer contact area.

In summary, the nonlinear damage and failure process of the SFSRCB under impact load is as follows: In the local response stage, due to the action of the main peak value of impact force, several fine cracks are formed in the local mid-span area of the beam. In the overall deformation stage, the mid-span displacement gradually increases, and reaches the peak value. At this stage, the energy consumption of reinforcement deformation gradually increases, and the micro cracks on the beam surface are fully developed, as manifested by the increase in crack width and length. In the rebound stage, the mid-span displacement gradually decreases from the peak value to the residual displacement value. At this stage, the specimen gradually rebounds upward, and the width of cracks on the surface decreases.

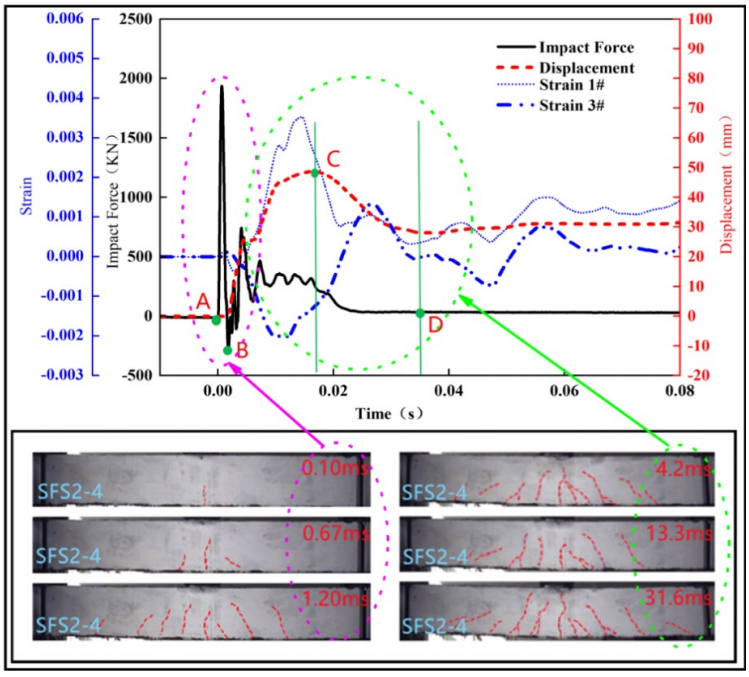

Fig. 3 Impact response and failure history of SFS2-1

3.2 Time history analysis of impact force and mid-span displacement

In Section 3.1, the dynamic damage mechanism of SFSRCB has been emphatically analyzed, and the dynamic failure process of the beam body is divided into the local resistance stage, overall deformation stage and rebound stage. To further elucidate the dynamic response of the SFSRCB, this section will analyze the influence of impact energy, impact mass and impact mode on the impact force and mid-span displacement of the SFSRCB under impact load. In this test, the data of six SFSRCBs are measured, and the time history curves of impact force and mid-span displacement are collected and organized, as shown in Fig. 4. The corresponding special impact response data are shown in Fig. 5.

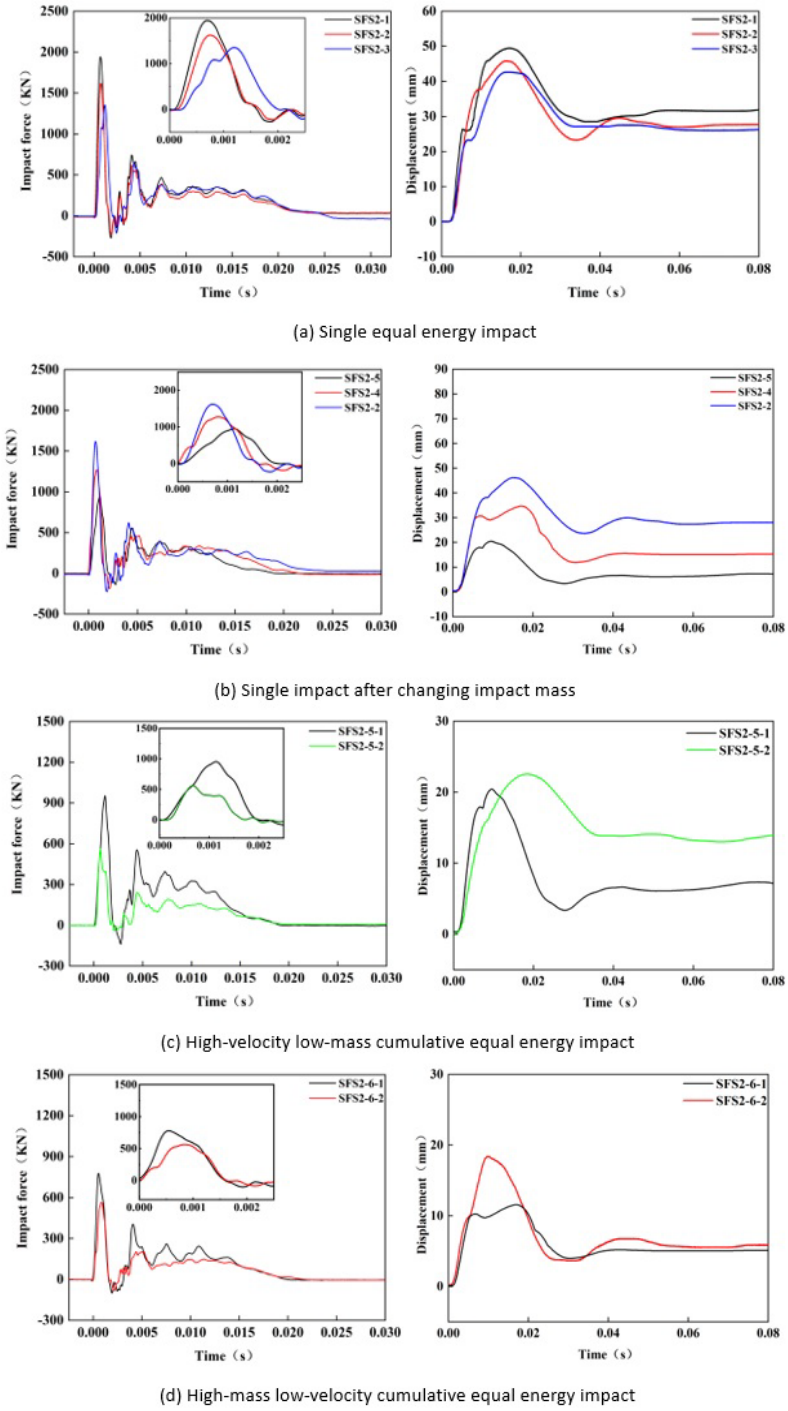

(a) Single equal energy impact

(b) Single impact after changing impact mass

(c) High-velocity low-mass cumulative equal energy impact

(d) High-mass low-velocity cumulative equal energy impact

Fig. 4 Time history curve of impact force and mid-span displacement of each specimen

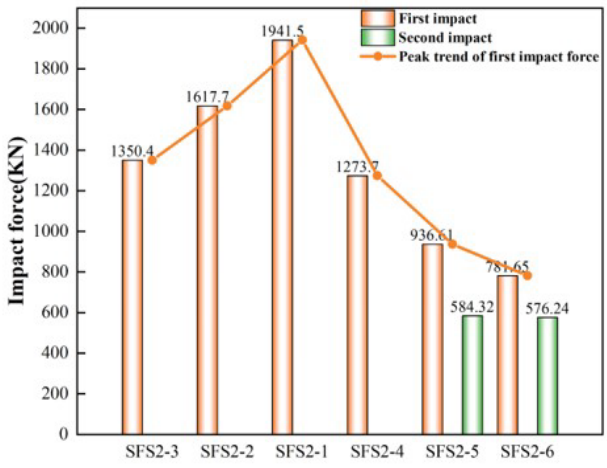

(a) Data of peak impact force

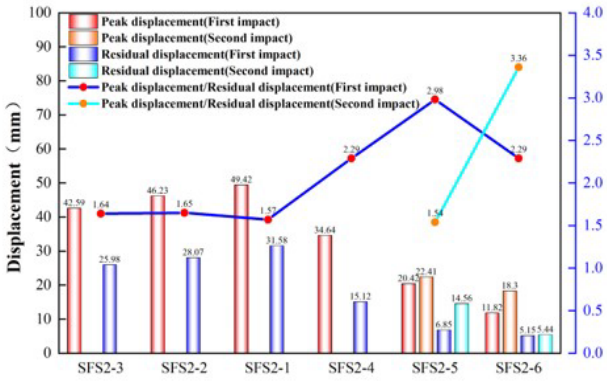

(b) Data of mid-span displacement peak value and residual displacement

Fig. 5 Impact response data of each specimen

It can be seen from the figure that, when the beams of Group A (SFS2-3, SFS2-2 and SFS2-1) are subjected to a single equal energy impact, with the gradual reduction of impact mass (800–400 kg), then the impact velocity gradually increases (5.38–7.66 m/s), and the peak impact force increases by 19.8% and 20.1%, respectively. For the beams of Group B (SFS2-5, SFS2-4 and SFS2-2), when the impact velocity is equal, then the impact mass increases from 200 kg to 400 and 600 kg, and the peak impact force increases by 36.0% and 27.0%, respectively. Compared with the research of Zhou et al. (2021), when the impact mass is 800 kg, the impact velocity increases from 4.36 m/s to 6.14 and 7.64 m/s, and the peak impact force increases by 40.39% and 41.15%, respectively. The above data show that, compared with the impact mass, the impact velocity has a greater impact on the peak impact force in the local resistance stage of the beam.

When the beams of Group A are impacted by different combinations of impact mass and velocity, particularly when the impact velocity gradually increases, then the peak mid-span displacement increases by 8.5% and 6.9%, respectively. When the impact velocity of the Group B beams remains unchanged, then, with the increase of impact mass, the peak mid-span displacement increases by 69.6% and 33.5%, respectively, and the residual displacement increases by 120.7% and 85.6% accordingly. Compared with the research of Zhou et al.(2021), when the impact mass remains unchanged, then the impact velocity increases successively, the peak mid-span displacement increases by 50.6% and 33.4%, and the residual displacement increases by 81.6% and 52.5%, respectively. From these observations it is clear that, compared with the increase of impact mass, increase in the impact velocity will lead to a greater peak value of mid-span displacement in the overall deformation stage, and in turn more serious impact damage to the beam. When the beams of Group A are subjected to equal energy impact, the ratio of peak mid-span displacement to residual displacement remains basically unchanged with the increase of impact velocity. When the impact velocity of the Group B beams

remains unchanged, then the impact mass increases to 3 times successively, and the ratio of peak mid-span displacement to residual displacement decreases by 23.15% and 27.9%, respectively. When the impact mass remains unchanged, then the impact velocity increases to 1.75 times successively, and the ratio of peak mid-span displacement to residual displacement decreases by 15.7% and 14.3%, respectively. The above data reveal that the impact energy is the main factor affecting the deformation resilience of the beam, and the impact velocity has a greater impact than the impact mass.

For the beams of Group C (SFS2-5 and SFS2-6), under the cumulative equal energy impact, the peak ratios of the second and first impact forces of SFS2-5 and SFS2-6 specimens are 62.38% and 73.72%, respectively. This indicates that the impact velocity has a greater impact on the cumulative impact stiffness loss of the specimens than the impact mass. During the first and second impacts of the SFS2-5 specimens, the ratio of peak mid-span displacement peak to residual displacement is 2.98 and 1.54, respectively. During the first and second impact of SFS2-6 specimens, the ratio of peak mid-span displacement peak to residual displacement is 2.29 and 3.36, respectively. This indicates that under the cumulative equal energy impact, the high-velocity low-mass(200kg,6.22m/s) impact has a greater impact on the damage and deformation recovery ability of the beam than the low-velocity high-mass(400kg,4.34m/s) impact.

3.3 Failure form

The failure mode of each specimen after being impacted by the drop hammer is shown in Fig. 6 below. It should be noted that since the micro cracks in the physical image are difficult to observe, the on-site sketch observation diagram is drawn and analyzed, and the failure modes of SFSRCB specimens are studied and compared. The black and gray curves respectively represent the wide cracks and fine cracks that can easily be observed.

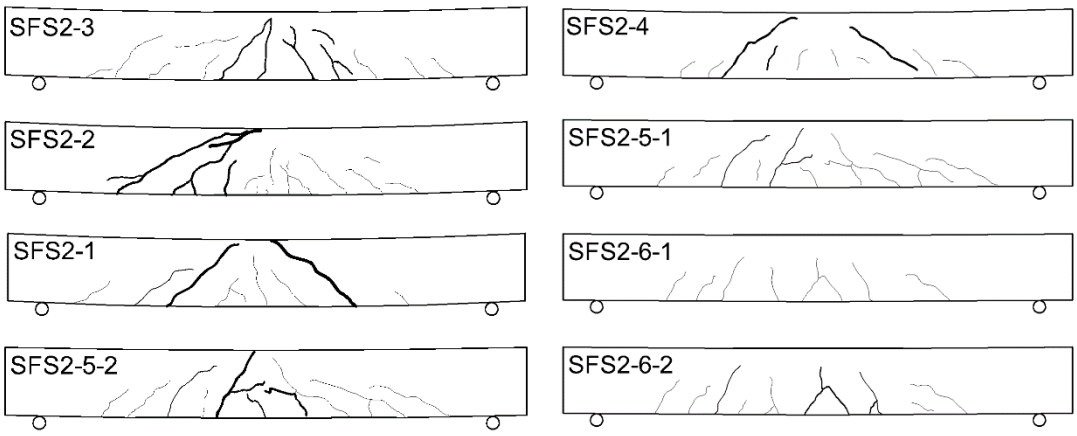

Fig. 6 Damage and failure of each specimen

It can be seen from the figure that there is no obvious concrete crushing on the impact contact surface among all of the SFSRCBs. SFS2-1, SFS2-2 and SFS2-3 are the three beam specimens, and are impacted by equal energy. Among these three beams, SFS2-1 is impacted by the maximum impact velocity and minimum impact mass. Diagonal shear oblique cracks are generated at an angle of approximately 45° from the impact point to the lower part of both sides of the support, and run through the entire section from bottom to top. Several fine vertical cracks are generated between the middle and lower parts of the span and the impact point. The mid-span residual deflection of the specimen is about 32 mm. The failure form of the specimen is local shear failure. As for specimen SFS2-2, the impact velocity decreases, and the impact mass increases. A shear oblique crack is generated from the impact point to the lower part of the support, while multiple fine short cracks are generated from the beam bottom to the impact point. The overall crack distribution

area increases, and the mid-span residual deflection is roughly 30 mm. The failure form is overall shear failure. Specimen SFS2-3 is impacted by the smallest impact velocity and the largest impact mass. The local area of the specimen consists of vertical cracks and 60° oblique cracks. The number of cracks is large and densely distributed, the distribution range of cracks is further enlarged, and the failure form of the specimen is clearly bending shear failure.

The impact velocities of SFS2-5, SFS2-4 and SFS2-2 beams are the same, and the impact mass gradually increases from 200 to 600 kg. It can be seen that the overall failure mode of the specimen remains basically unchanged. With the increase of impact mass, the crack of SFSRCB extends from bottom to top, the crack distribution area enlarges, and the crack number increases. SFS2-5 and SFS2-6 are impacted twice with equal energy. SFS2-5 exhibits many bending shear cracks in local areas upon the first impact, while the beam surface of SFS2-6 is almost completely covered by vertical cracks, thus indicating that the impact velocity has a significant impact on the shear effect of the specimen. The crack of the specimen upon the second impact basically develops along the original crack. In contrast, the residual deflection of the SFS2-5 specimen reaches 14.56 mm, while that of SFS2-6 is only 5.44 mm, thus indicating that the impact velocity leads to a more serious impact damage to the beam during the cumulative equal energy impact.

SFS2-5 and SFS2-6 are impacted with equal energy, and the total energy is equal to the single impact energy of SFS2-4. In contrast, the total deformation of SFS2-5 and SFS2-6 is higher than that of SFS2-4, while that of SFS2-5 is also higher than that of SFS2-4, but that of SFS2-6 is lower than that of SFS2-4. In addition, after the two impacts, SFS2-5 forms a through crack, and its damage degree is higher than that of SFS2-4. There are many micro cracks in SFS2-6, and most are vertical cracks, without through cracks. In general, the damage degree of specimen SFS2-6 is lower than that of SFS2-4. The above results suggest that when the impact energy is consistent, the overall damage of high-velocity low-mass(200kg,6.22m/s) cumulative impact is more serious than that of single impact, while the overall damage of high-mass low-velocity(400kg,4.34m/s) cumulative impact is less significant than that of single impact.

4 FINITE ELEMENT ANALYSIS AND EXTENSION

The emergence of numerical simulation software has greatly solved the problem faced during advancement of researchers in various fields. ABAQUS is one of the commonly used commercial finite element software available at this stage. In particular, Explicit analysis module show strong nonlinear function in the impact resistance research of RC structures. Jin et al. (2020) also applied the software for academic research. In this paper, ABAQUS software is used to establish the numerical model of SFSRCB with steel fiber content of 2.0%, and to extend the research on SFSRCB under different impact conditions.

4.1 Modeling process

Based on the test, this paper establishes the finite element model of SFSRCB impacted by drop hammer through ABAQUS/Explicit analysis module, as shown in Fig. 7. The entire drop hammer is simplified into a rigid cylinder, and the mass and initial velocity are applied. A simply supported beam is adopted as the boundary constraint mode at both ends of the beam. The reinforcement is simulated by three-dimensional truss element T3D2, while the concrete, support and drop hammer are simulated by three-dimensional solid element C3D8R. Considering the hourglass control, the reinforcement is embedded into the concrete to achieve perfect bonding (Jin et al., 2020).

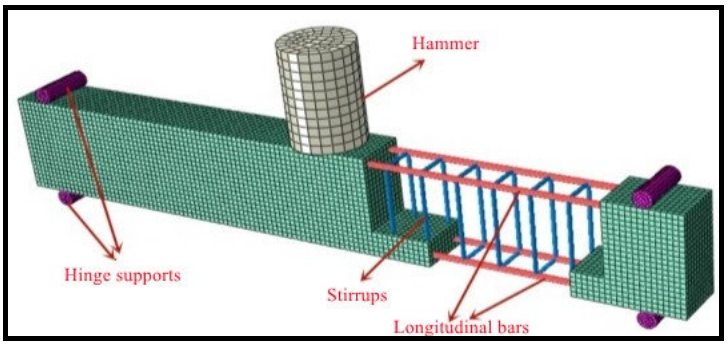

Fig. 7 Finite element model

4.2 Material constitutive model

(1) Drop hammer and base: The elastic model is used to describe its mechanical behavior according to the mechanical properties of steel.

(2) Ordinary C40 concrete: The concrete damage plastic model (CDP) provided in ABAQUS is used for simulation, with consideration to the nonlinear behavior of concrete. The tensile and compressive stress-strain relationship curve of concrete under uniaxial cyclic load is shown in Fig. 8. The mechanical properties of concrete in the elastic stage are calculated based on the initial elastic modulus of the CDP model, and the parameter input of the CDP model is shown in Table 3. For the characterization of the mechanical properties of concrete in the damage plastic stage, the damage evolution parameters based on damage factors introduced in GB50010-2010 (2015) are adopted, and the dynamic strain rate effect of concrete is considered (Plauk,1982).

Table 3 Concrete material parameters based on the CDP model

Expansion angle ψ	Eccentricity η	Biaxial to uniaxial compressive strength ratio f_{b0}/f_{c0}	K	Viscosity coefficient μ
30^0	0.1	1.16	0.66667	0.00005

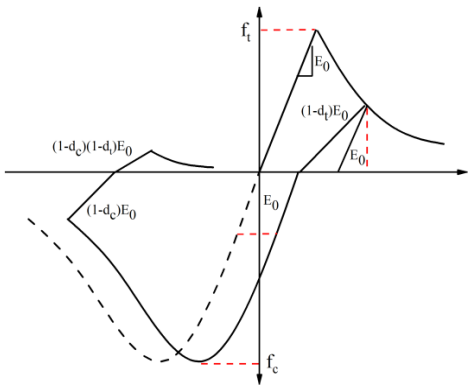

Fig. 8 Uniaxial tension-compression curve of plastic damage

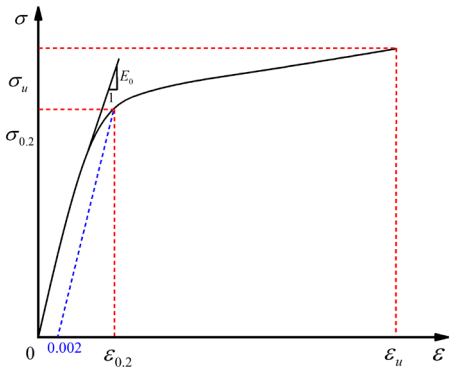

Fig. 9 Constitutive model of stainless steel

(3) Steel fiber reinforced concrete: In this paper, the macro modeling method is used to simulate the steel fiber reinforced concrete. The macro method does not directly simulate the steel fiber, and instead only considers the influence of adding steel fiber on the strength of ordinary concrete. The specific method is as follows: The measured value of the compressive strength of steel fiber reinforced concrete is obtained through the compression test on steel fiber reinforced concrete test blocks with different fiber contents, and the tensile strength is converted according to *Steel Fiber Reinforced Concrete* (JG/T 472-2015), in combination with the type and content of steel fiber. Next, the stress-strain curves of steel fiber reinforced concrete with different steel fiber contents are obtained with the same method as that used for ordinary concrete. This macro simulation method may be regarded as amplifying the strength of ordinary concrete.

(4) Stainless-steel reinforcement: For the selection of constitutive model of stainless steel reinforcement, this paper refers to the research work of Yousuf et al. (2013), and applies the stainless steel constitutive relationship proposed by Rasmussen and Kim. (2003) for simulation. The constitutive model is shown in Fig. 9.

4.3 Discussion and verification of modeling methods

Table 4 shows the comparative data of the key impact response parameters of six specimens. It can be seen from the table that the macro simulation method is suitable for the dynamic response simulation of the SFSRCBs. In addition, taking specimen SFS2-1 as an example, the test and numerical simulation values are compared. It can be seen from Fig. 10 that the macro simulation curve is in high agreement with the development trend of impact force and mid-span displacement in the test.

Table 4 Comparison of impact response values between test and finite element

Specimen No.	Peak impact force (kN)		Relative error (%)	Peak value of mid-span displacement (mm)		Relative error (%)
	Simulation	Experiment		Simulation	Experiment	
SFS2-3	1366.8	1350.4	+1.2	40.6	42.59	-4.9
SFS2-2	1684.7	1617.7	+4.1	45.1	46.23	-2.5
SFS2-1	1974.6	1941.5	+1.7	47.8	49.42	-3.4
SFS2-4	1199.4	1273.7	-6.2	34.2	34.64	-1.3
SFS2-5	895.51	936.61	-4.6	21.9	20.42	+7.2
SFS2-6	799.74	781.65	-2.3	12.2	11.82	+3.2

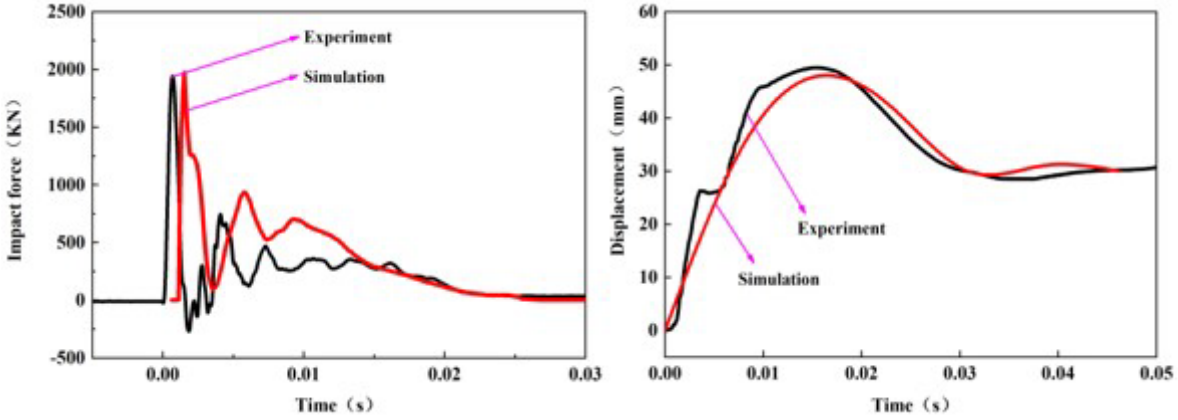

Fig. 10 Comparison between SFS2-1 test and macro numerical simulation

5 IMPACT BEARING CAPACITY ANALYSIS AND IMPACT DAMAGE EVALUATION OF SFSRCB

5.1 Experimental research of Tachibana **(Tachibana et al., 2010)** and Kishi **(Kishi et al., 2001)**

The energy dissipation methods of the beam under impact load include overall large deformation cracking and local concrete damage energy dissipation on the impact surface. Tachibana et al. (2010) evaluated the test results for the impact load characteristics and impact performance of RC beams with different shear-to-bending deformation ratios. The correlation of characteristic quantities such as impact energy (E_0), impact mass (M_2), duration of impact force (Δ_t), impulse (I_t) and bending bearing capacity (P_u) were studied. Then, based on the relationship between impact energy and static bending bearing capacity, the empirical formula for calculating the maximum mid-span deflection (Δ_{max}) of beam under impact load was estimated (Tachibana et al., 2010):

$$\Delta_{max}=0.522\frac{E_0}{P_u} \tag{1}$$

Kishi et al. (2001) conducted vertical impact tests on 36 rectangular simply supported beams with different section sizes, reinforcement ratios and concrete compressive strengths by using a drop hammer testing machine, and fitted the fitting relationship expression between the static bending bearing capacity and maximum mid-span displacement (Δ_{max}) and average residual displacement (Δ_{rd}) through mass test data(Kishi et al., 2001):

$$P_u=0.63\frac{E_0}{\Delta_{max}} \tag{2}$$

$$P_u=0.42\frac{E_0}{\Delta_{rd}} \tag{3}$$

5.2 Maximum mid-span displacement formula of SFSRCBs under impact load

The above calculation formula is only applicable to ordinary reinforced concrete beams. At present, no researchers have studied the mid-span deflection formula of steel fiber stainless steel reinforced concrete beams. Based on the above research results, the present paper deduces the empirical formula for calculating the mid-span deflection of an SFSRCBs with fiber content of 2.0%, establishes the corresponding finite element model of the SFSRCBs, changes the parameters such as impact mass, impact velocity and stirrup ratio, and fits the mid-span deflection formula of the SFSRCBs with steel fiber content of 2.0% under impact load in combination with the test results of the SFSRCBs and the test results of Zhou et al. (2021), referring to the research methods of Tachibana, Kishi and others:

$$\Delta_{\max}=0.427\frac{E_0}{P_u} \tag{4}$$

$$\Delta_{rd}=0.249\frac{E_0}{P_u} \tag{5}$$

From the comparison of Formulas (1), (2) and (3) with Formulas (4) and (5), it can be seen that under the same impact parameters, the constant coefficients in Formulas (4) and (5) are small. In other words, compared with ordinary RC beams, SFSRCBs exhibit high ductility and resilience, and improve the ability of resisting impact deformation. Through the analysis and comparison of test data of relevant researchers, test data and finite element simulation data, as shown in Fig. 11, it is found that the dispersion degree is low by comparing the values calculated by Formulas (4) and (5) with the test data and simulation results.

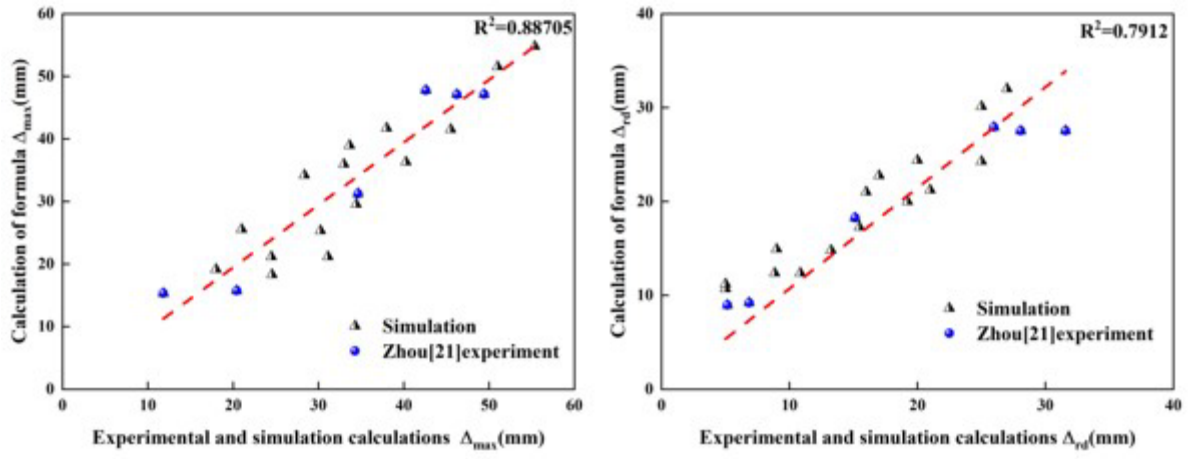

Fig. 11 Comparison between measured and simulated deflection value and calculated deflection value of Formula (4)

5.3 Ultimate mid-span elastic displacement of SFSRCBs under impact load

Calculation of the maximum elastic displacement of the beam under impact load: It is assumed that the deformation curve of the beam under impact load maintains a specific shape. In addition, it is considered that the total mass of the beam can be equivalent to a single-degree-of-freedom (SDOF) concentrated mass point, and the overall equivalent stiffness and damping of the beam are simulated by the spring and damper system. Next, the measured curve of impact

force time history is applied to the single mass point system to calculate the overall response of the mass point (Zhao, 2017). The simplified diagram of simply supported beam under the impact of drop hammer is shown in Fig. 12 below.

The hammer-beam impact dynamic response system is simplified into a mass-spring-damping system (without considering contact stiffness and contact damping). The elastic vibration law of rectangular long beam under impact is calculated by the vibration equation on the basis of structural dynamics. The basic assumptions are as follows: The beam body is considered as a SDOF system, while considering the influence of beam and drop hammer mass. The mass body M_2 simulates a rigid drop hammer. The equivalent mass of the beam body is M_1, and the resistance stiffness of the beam is equivalent to a spring body with stiffness K. For the value of K and the calculation method of equivalent SDOF point mass of beam M_1, see Reference (Zhao, 2017) , and the self-damping is simplified to viscous damping with damping value of Q. The maximum elastic displacement of the beam under impact load is calculated by solving the calculation results of the model.

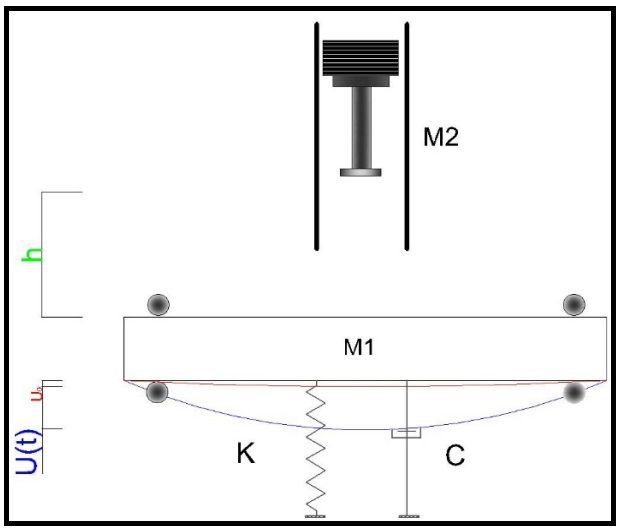

Fig. 12 Mass-spring-damping system model

Considering the influence of gravity of the beam and hammer on the deflection, the model takes the static equilibrium position of the $M_1 - K$ system as the origin. During the vibration process of the system, the static equilibrium position under the joint action of $M_1 + M_2$ is $u_0 = M_2 g / K$. The rising height of mass body M_2 (simulated drop hammer) is recorded as h, the free fall is released along the track, and the mass body contacts and collides with the equivalent SDOF mass $M_1 = \frac{\rho bh}{3}(L_0 + (L - L_0)^3 / L_0^2)$ (Zhao, 2017) at an initial velocity of $v_0 = \sqrt{2gh}$. The initial kinetic energy before impact is E_k, and the beam is within the elastic range after impact. Therefore, it can be considered that, before the beam reaches plastic deformation, the drop hammer is in close contact with the beam, and the two mass blocks move at the same speed v_t. Then, according to the conservation of momentum, the following can be obtained:

$$v_t = \frac{M_2}{M_1 + M_2}\sqrt{2gh} \tag{6}$$

Therefore, the entire model system generates the time history curve of the beam-hammer common response displacement due to the excitation of the beam body by the free fall of the drop hammer, assumed as $u(t)$. The impact process is completed in an instant and the damping ratio of the reinforced concrete structure is generally less than 5%, thus the equivalent damping of the beam body Q is determined according to the research of Fujikake et al. (2009). The effect of damping is ignored in the process of instantaneous forcing, i.e., Q=0, and the beam body vibrates freely after the impact. The influence of damping on the attenuation response is considered. At this time, the difference between the forced vibration of the damped and undamped system is quite small. The motion solution of the undamped system can be used to replace the motion solution of the damped system.

According to the D-Alembert principle, the vibration equilibrium equation of the entire system is established, as follows:

$$（M_1 + M_2）（\ddot{u}(t) - \ddot{u}_0）+K(u(t) - u_0) = 0 \tag{7}$$

Next, set up the general solution of the equation:

$$u(t) = p\cos\omega_n t + q\sin\omega_n t, \quad \omega_n = \sqrt{\frac{K}{M_1 + M_2}} \tag{8}$$

The special solution is the solution satisfying Formula (7), recorded as $u_p(t)$. Set the special solution as $u_p(t) = C\sin\omega t + D\cos\omega t$, and substitute it into Formula (7) to obtain $D = 0$, $C = u_0 \frac{1}{1 - \omega / \omega_n}$. The complete solution of the motion equation is the sum of the general solution and the special solution. Then substitute the initial displacement and initial velocity into the equation, as follows:

$$u(t) = -\frac{M_2 g}{K}\cos\omega_n t + [M_2\sqrt{\frac{2gh}{K(M_1 + M_2)}}]\sin\omega_n t + u_0 \tag{9}$$

5.4 Dynamic calculation analysis and impact damage evaluation of SFSRCBs

In terms of parameter selection, the beam body is simplified into a triangular model composed of two rigid bars and plastic hinges. Only the elastic stage in which the concrete does not crack is considered. According to the domestic requirements of concrete structure design code, the short-term stiffness of rectangular section of the SFSRCB is taken as $B = \frac{E_s A_s h_0^{\ 2}}{1.15\psi + 0.2 + 6\alpha_E \rho_t}$, where h_0 =265 mm, the effective height of the beam section; A_s =402 mm^2, the cross-

sectional area of longitudinal tensile reinforcement; ψ is the strain non-uniformity coefficient of longitudinal tensile reinforcement between cracks, taken as 1.0 after calculation; α_E is the ratio of elastic modulus of reinforcement to elastic modulus of concrete, i.e., E_s / E_c; and ρ_t is the reinforcement ratio of longitudinal tensile reinforcement. In addition, the equivalent stiffness of the beam body is calculated according to structural mechanics, $K = 48B / L_0^3$.

In view of the complex elastoplasticity and instantaneity of reinforced concrete beams subjected to external strong impact, the ratio of the maximum displacement $\Delta_{\max}$ to the maximum elastic displacement $U_{\max}$ generated in the mid-span of the beam during the impact process is defined as the damage evaluation index of the beam. Due to the fact that the equivalent stiffness value of the beam is much greater than the mass value of the drop hammer, the influence of the static equilibrium position $u_0 = M_2 g / K$ is almost negligible. The $u_{\max} = M_2\sqrt{\frac{2gh}{K(M_1+M_2)}}$, next, calculation is performed in combination of Formulas (4) and (9), and the expression of damage factor α associated with impact energy, static load bending bearing capacity and beam-hammer mass ratio is proposed:

$$\alpha=\frac{\Delta_{\max}}{U_{\max}}=0.427\sqrt{\frac{K}{2}\left(\frac{M_1}{M_2}+1\right)}\frac{\sqrt{E_0}}{P_{\mathrm{u}}} \tag{10}$$

For different impact conditions, the maximum mid-span deflection measured in this test is added Formula (10) and compared with the theoretical calculation results. It can be seen from Table 5 that the maximum elastic deflection of the beam body exhibits obvious differences during the different impact conditions. With the increase of impact energy, the maximum elastic deflection of the beam body increases significantly. For the equal energy impact test, increasing the impact mass is conducive to improving the maximum elastic deflection of the beam body, particularly under low-energy impact. Combined with the damage diagram of beam in Fig. 6, the damage degree of the beam can be preliminarily determined. When the damage factor α=0.87~0.94 (slight damage), it is held that the beam has not yet entered the plastic stage, and has undergone slight bending failure. When α=1.20~1.44 (moderate damage), the corresponding beams have mainly been damaged by bending shear. Finally, when α=1.46~1.52 (severe damage), the beam damage has gradually developed from overall shear failure to local shear failure. Subsequent research can be verified by a large number of experiments and finite element.

Table 5 Results of dynamic calculation

Specimen No.	K (10^7N/m)	P_u (kN)	V_0 (m/s)	M_2 (kg)	$U_{\max}$ (mm)	$\Delta_{\max}$ (mm)	α	Failure mode
SFS2-1	1.97	104.64	7.66	400	31.41	47.88	1.52	Local shear failure
SFS2-2	1.97	104.64	6.21	600	32.34	47.21	1.46	Overall shear failure
SFS2-3	1.97	104.64	5.38	800	32.84	47.24	1.44	Bending shear failure
SFS2-4	1.97	104.64	6.14	400	25.65	30.77	1.20	Bending failure
SFS2-5	1.97	104.64	6.22	200	16.76	15.79	0.94	Bending failure
SFS2-6	1.97	104.64	4.34	400	18.14	15.37	0.87	Bending failure

6 CONCLUSION

In this paper, drop hammer impact test is conducted on six SFSRCBs with steel fiber content of 2.0%, so as to study the nonlinear dynamic response of the beam to the impact energy at each stage. The deflection expression and damage evaluation method of the SFSRCBs under impact load are discussed in combination with numerical modeling and the dynamic analysis method. The main conclusions of the study are as follows:

(1) Compared with the impact mass, the impact velocity is the most sensitive factor affecting the peak value of impact force in the local response stage and the peak value of mid-span displacement in the overall deformation stage. The impact energy is the main factor affecting the deformation resilience of the beam, and the impact velocity has a greater impact than the impact mass. Under the cumulative equal energy impact, the high-velocity low-mass(200kg,6.22m/s) impact lead to greater loss of cumulative impact stiffness of the beam and weaken the deformation recovery ability of the specimen.

(2) Under the action of single equal energy impact, the shear effect of beam becomes increasingly significant with the increase of impact velocity. When the total energy of cumulative impact is consistent with that of single impact, then the overall damage degree of the high-velocity low-mass cumulative impact on the specimen is greater than that of single impact, and the overall damage degree of high-mass low-velocity cumulative impact on the beam is the lowest.

(3) In this paper, according to the test and simulation data, the empirical formula of mid-span deflection of SFSRCBs under impact load is derived based on dynamic theory. Finally, the impact damage evaluation factors of SFSRCBs related to impact energy, static bending bearing capacity and beam-hammer mass ratio are proposed.

7 DISCUSSION

It is worth noting that in this paper, only six SFSRCBs with steel fiber content of 2% are subjected to impact tests under different impact energies, and there is a lack of impact test analysis on SFSRCBs with different steel fiber contents. In other words, the application scope of dynamic damage evaluation factors of SFSRC beamsSFSRCBs remains quite limited. Therefore, in subsequent research it will be necessary to carry out additional impact tests on SFSRCBs with different fiber contents, and this issue must be studied in depth through combination with finite element and theoretical analysis.

ACKNOWLEDGMENTS

The author(s) disclosed receipt of the following financial support for the research, authorship, and/or publication of this article: The research findings described in this paper was sponsored by the Characteristic Innovation Project of Guangdong Universities (Project Number: 2020KTSCX128), and the Engineering technology research and Development Center for intelligent marine and terrestrial geotechnical material in Foshan for their helps in this work.

Author's Contributions: Conceptualization, Xiwu Zhou, Bo Wang, Wen Zhang; Methodology, Xiwu Zhou, Bo Wang, Jingdong Liu; Writing - original draft, Xiwu Zhou and Bo Wang; Writing - review & editing, Xiwu Zhou, Bo Wang, Wen Zhang; Resources, Xiwu Zhou and Xiaolu Deng; Supervision, Xiwu Zhou.

Editor: Marcílio Alves

References

Zhang, Y. L., Su, R. K. L. (2020). Corner cracking model for non-uniform corrosion-caused deterioration of concrete covers. Construction and Building Materials. 234: 117410.

Zhang, W. M., Chen, S. H., Liu, Y. Z. (2017). Effect of weight and drop height of hammer on the flexural impact performance of fiber-reinforced concrete. Construction and Building Materials. 140: 31-35.

Song, M., Wang, Z. Y., Zhang, J., Ma, G., Wang, Z. H. (2021). The influence from steel bar on concrete fracture behavior under different impact velocities. STRUCTURAL CONCRETE. 22(6): 3510-3525.

Fu, Y. Q., Yu, X. L., Dong, X. L., Zhou, F. H., Ning, J. G., Li, P., Zheng, Y. X. (2020). Investigating the failure behaviors of RC beams without stirrups under impact loading. International Journal Of Impact Engineering. 137.

Xu B, Zeng X. (2015). Tests for dynamic behaviors of deep RC beams under impact loadings . Journal of Vibration and Shock. 34(04): 6-13.

Zhang, G. X., Xu, S. X., Xie, H. B., Zhou, X. W., Wang, Y. F. (2017). Behavior of stainless steel–reinforced concrete piers under lateral impact loading. Advances in Mechanical Engineering. 9(5): 2071940081.

Zhang, G. X., Xu, S. X. (2017a). Test study on the impact damage performance of stainless steel reinforced concrete . AIP conference proceedings. 1829(1).

Wu, B., Xu S. X. (2020). Experimental study on damage evaluation of stainless steel–reinforced concrete piers under lateral impact. Advances in Mechanical Engineering. 12(5).

Rabi, M., Cashell, K. A., Shamass, R. (2019). Flexural analysis and design of stainless steel reinforced concrete beams. Engineering Structures. 198.

Zhou, X. W., Zhang, W. C., Gao, Y. S., Zhang, G. X., Xiong, R. S. (2020). A Comparative Test Study of the Impact Performances of Stainless-Steel Rebar Equal-Strength Replacement Piers. International Journal of Steel Structures. 20(1): 67-79.

Zhou, X. W., Zhang, R. C., Zhang, G. X., Wang, X. Y. (2019). Experimental Study on Impact Mechanical Properties of RC Beams Replaced by Stainless Steel Bars with Constant Cross Section. Journal of Xinyang Normal University(Natural Science Edition). 32(03): 487-491.

Leppanen, J., Johansson, M., Grassl, P. (2020). On the dynamic response of reinforced concrete beams subjected to drop weight impact. Finite Elements In Analysis And Design.180.

Ulzurrun, G. S. D., Zanuy, C. (2017). Enhancement of impact performance of reinforced concrete beams without stirrups by adding steel fibers. Construction and building materials. 145: 166-182.

Dou, G. Q., Du, X. L., Li, L. (2015). Experiment on Behavior of Reinforced Concrete Beams with Steel Fiber Under Impact Load. Journal of Tianjin University(Science and Technology). 48(10): 864-872.

Lee, J. Y., Shin, H. O., Yoo, D. Y., Yoon, Y. S. (2018). Structural response of steel-fiber-reinforced concrete beams under various loading rates. Engineering Structures. 156: 271-283.

Tachibana, S., Masuya, H., Nakamura, S. (2010). Performance based design of reinforced concrete beams under impact. Natural Hazards and Earth System Sciences. 10(6): 1069-1078.

Kishi N, Nakano O, Matsuoka K G, et al. (2001). Experimental Study on Ultimate Strength of Flexural-Failure-Type RC Beams under Impact Loading.

Zhao, D. B., Yi W. J. (2015). Anti-impact behavior and design method for RC beams[J]. Journal of Vibration and Shock. 34(11): 139-145.

Li, R. W., Zhou, D. Y., Wu, H. (2020). Experimental and numerical study on impact resistance of RC bridge piers under lateral impact loading[J]. Engineering failure analysis. 109.

Zhao, W. C., Qian, J., Zhang, W. N. (2019). Performance and damage evaluation of RC beams under impact loading[J]. Explosion and Shock Waves. 39(01): 111-122.

Zhou, X. W., Zhang, W., Wang, X. Y. (2021). Experimental study of the mechanical properties of steel fiber stainless-steel reinforced concrete (SFSRC) beams under low velocity impact conditions. Advances in Mechanical Engineering. 13(9).

Code for design of concrete structures (GB 50010-2010) (2015). National standards of People's Republic of China.

Li, H. W., Chen, W. S., Hao, H. (2019). Dynamic response of precast concrete beam with wet connection subjected to impact loads. Engineering Structures. 191: 247-263.

Liu, F., Luo, Q. Z., Jiang, Z. G. (2015). Dynamic responses and failure mechanism of rc beams to low velocity impact. Engineering Mechanics. 32(05): 155-161.

Cai, J., Yu, Y., Chen, Q. J., Li, Y. N., Ye, J. B. (2019). Parameter study on dynamic response of concrete filled square tube under lateral impact. Journal of Central South University (Science and Technology). 50(02): 409-419.

Jin, L., Lan, Y. C., Zhang, R. B., Du, X. L. (2020). Impact resistances of RC beams at/after high temperature: Meso-scale analysis (in Chinese). Sci Sin-Phys Mech Astron, 50(02): 120-130.

Plauk G.. (1982). Concrete structures under impact and impulsive loading.

Yousuf, M., Uy, B., Tao, Z., Remennikov, A., Liew, J. Y. R. (2013). Transverse impact resistance of hollow and concrete filled stainless steel columns. Journal of Constructional Steel Research. 82: 177-189.

Rasmussen, Kim. J. R. (2003). Full-range stress–strain curves for stainless steel alloys. Journal of constructional steel research.59(1): 47-61.

Zhao, D. B. (2017). Response characteristics and design method of reinforced concrete beams under impacting load. Hunan University.

Fujikake, K., Li, B., Soeun, S. (2009). Impact Response of Reinforced Concrete Beam and Its Analytical Evaluation. Journal of structural engineering (New York, N.Y.). 135(8): 938-950.